INTERNATIONAL JOURNAL OF AUTOMOTIVE AND MECHANICAL ENGINEERING
ISSN: 2229-8649 e-ISSN: 2180-1606
VOLUME 23, ISSUE 3, 2026, 13756 - 13772
DOI: https://doi.org/10.15282/ijame.23.3.2026.2.1038

RESEARCH ARTICLE

Design, prototype verification, finite-element assessment, and direct-cost evaluation of a wheelchair-accessible low-speed electric campus buggy for inclusive mobility

Zammeri Abd Rahman[1]*, Saiful Bahri Mohamed[1], Rodianah Alias[2], Mohd Sobri Hamid[1], Mohd Shahir Kasim[1], W Noor Fatihah W. Mohamad[1], Wan Ahmad Luqman Ellias Wan Saidi[2], Ahmad Syauqi Azlan[2] and Madihah Maharof[3]

[1]Design Optimisation & Manufacturing Research Group, Faculty of Innovative Design and Technology, Universiti Sultan Zainal Abidin, Kampus Gong Badak, 21300 Kuala Nerus, Terengganu, Malaysia
[2]Faculty of Innovative Design and Technology, Universiti Sultan Zainal Abidin, Kampus Gong Badak, 21300 Kuala Nerus, Terengganu, Malaysia
[3]Department of Mechanical and Production Engineering, Islamic University of Technology, Board Bazar, Gazipur-1704, Bangladesh

Abstract - Mobility between campus buildings can remain inaccessible even when individual facilities are barrier-free. This study developed and verified a wheelchair-accessible, low-speed electric campus buggy, in which boarding access and manufacturability in workshops were considered from the conceptual stage. A requirements-driven Design Thinking process was combined with design-for-manufacture principles, CAD modelling, linear static finite-element analysis, full-scale prototype fabrication, controlled engineering tests, and direct-cost assessment. The prototype uses a welded AISI 1020 tubular ladder frame, continuous low anti-slip floor, open side access, multi-row seating, side guards, canopy, and detachable boarding ramp. Under the final static vertical load case, the chassis model produced a maximum von Mises stress of 140.0 MPa, maximum equivalent strain of 4.521×10^{-4}, maximum resultant displacement of 2.724 mm, and minimum safety factor of 2.511. The ramp remained elastic up to 180 kg, the mean stopping distance increased from 3.9 to 5.4 m at 15 km/h as the payload increased, and wheel lightening occurred at 24° and 21°under the driver-only and loaded conditions, respectively. The estimated energy consumption was 184–238 Wh/km, whereas the corrected direct prototype cost was MYR 36,363.16. The findings support continued controlled prototype development rather than service certification, with higher ramp proof loading, positive wheelchair securement, instrumented braking, direct centre of gravity measurement, and durability testing identified as priorities before routine use.

Article History
Received : 5 March 2026
Revised : 1 July 2026
Accepted : 14 August 2026
Published : 25 September 2026

Keywords
Inclusive campus mobility
Low-speed electric vehicle
Finite element analysis
Prototype verification
Energy–cost assessment

1. Introduction

Campus accessibility depends on more than just the accessibility of entrances to individual buildings. Students, staff, and visitors must also move between lecture spaces, offices, hostels, parking areas, workshops, and shared facilities. For wheelchair users, gradients, kerbs, uneven surfaces, and breaks in accessible routes can turn otherwise short journeys into practical barriers [1]–[3]. Low-speed vehicles (LSVs), including low-speed electric vehicles (LSEVs), are well suited for repeated travel on managed internal routes because their operating speed can be limited and their use can be coordinated with pedestrian-dominant areas [4]–[5]. Policy reviews of small electric mobility devices likewise emphasize the need to consider the operating context and user safety together [6]. An electric buggy alone does not solve the accessibility problem; boarding geometry, floor height, handholds, payload allowance, and stability must be addressed as part of the vehicle design. Wheelchair mobility research has addressed service provision and low-cost powered mobility [7]–[8], detachable drive modules and power-assist concepts [9]–[11], and other compact electric mobility platforms [12]–[13]. Together, these studies show that access, packaging, and propulsion decisions are closely linked. Design Thinking provides a structured way to translate user and context needs into engineering requirements [14], whereas design-for-manufacture and product-development methods encourage simpler geometry, repeatable assembly, and early evaluation of design limitations [15]–[16]. This approach is consistent with the authors' earlier workshop-scale development work. A modular magnetic jig showed the value of standardized interfaces and controlled positioning [17]; a portable drill guide combined CAD modelling, finite-element analysis, and physical prototype testing [18]; and a low-cost PC-based CNC platform demonstrated the practical benefits of modular construction and maintainable off-the-shelf hardware [19]. More recent structural optimization work used numerical evidence to target local stiffness improvements without simply increasing the structural mass [20]. Building on that experience, the present study treats wheelchair access as part of vehicle architecture rather than as a post-build modification. The objective of this study was to demonstrate a reproducible design-to-prototype route for a low-speed electric campus buggy that can be fabricated in a university workshop and evaluated using structural, functional, energy, and cost evidence. The revised manuscript therefore includes the design requirements, workshop constraints, finite element screening, fabrication controls, prototype tests, and direct-cost model into one engineering workflow.

***CORRESPONDING AUTHOR | Z. Abd Rahman** | ✉ zammeri@unisza.edu.my
© 2026 The Authors. Published by Universiti Malaysia Pahang Al-Sultan Abdullah Press. This is an open access article under the CC BY-NC 4.0 license

1.1 Related Work

Tubular and ladder-frame vehicle structures are commonly assessed based on their load paths, stiffness, local joint behavior, and manufacturability. Ladder-frame studies have examined cross-member geometry and stiffness [21], whereas combined simulation and experimental work have been used to refine light-commercial-vehicle chassis designs [22]. Recent reviews have identified material selection and section geometry as important design variables [23]. Experimental torsional stiffness studies and finite element analyses of student and off-road frames also provide useful precedents for locating weak regions before redesigning [24]–[25]. For compact electric vehicles, these structural questions directly interact with packaging and serviceability. Recent work on hollow-frame urban electric vehicles illustrates the value of lightweight, accessible frame layouts [26], whereas small electric vehicle development studies show the practical need to coordinate steering, drivetrain, and chassis decisions [27].

These findings are relevant to campus vehicles because a low operating speed does not eliminate the need for clear load paths, maintainable assemblies, and predictable handling. Affordability is the second design constraint. Earlier work on assistive-technology economics established the value of transparent cost–benefit reasoning [28], while more recent wheelchair selection research shows how technical and economic criteria can be considered together [29]. Parametric evaluation has also been applied to energy and refuelling strategies for small vehicles [30]. Recent electric-moped life-cycle studies quantify how component selection and end-of-life scenarios influence cost and environmental performance [31]–[32], and second-life battery research further demonstrates the economic importance of battery utilization beyond the first service [33]. What remains comparatively under-reported is a single prototype workflow that brings wheelchair access, DFM, structural assessment, physical verification, energy use, and direct fabrication cost together for a campus-scale LSEV.

2. Materials and Methods

A requirements-driven design-to-prototype methodology was adopted for this study. Instead of modifying an existing commercial cart, the study began with the campus access problem and translated it into a vehicle layout that could be built with the materials, equipment, and skills available in the institutional workshop. Design Thinking structured the requirement elicitation stage, DFM guided decisions on geometry and joining, and CAD-integrated linear-static finite element analysis provided an early structural screen. The completed prototype was then assessed through dimensional inspection, ramp loading and handling, braking, side slope stability, functional commissioning, energy estimation, and direct-cost analysis. The findings from each stage were used to identify changes for the next design iteration.

2.1 Design Thinking-Based Product Development Framework

travel close to pedestrians, stop often, and carry people with different mobility needs, access conditions were considered before the chassis layout was fixed. The first design notes therefore dealt with practical matters such as floor height, clear space at the entrance, ramp-assisted boarding, handhold position, expected payload, short route operation, and the capability of the workshop.

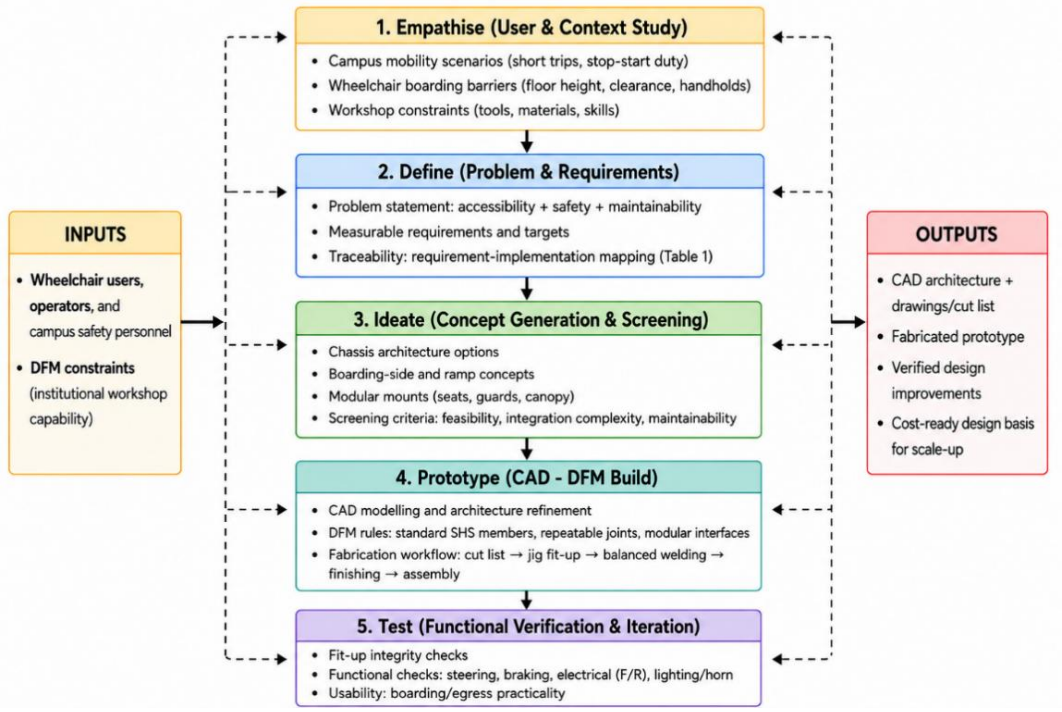


Figure 1. Design Thinking-based framework used to translate accessibility needs into prototype requirements, fabrication planning, and verification activities

These observations were organized through the five Design Thinking stages. In the Empathize stage, typical shuttle journeys and the likely boarding difficulties were reviewed. The Define stage converts these observations into engineering targets for access, payload, safety, manufacturability, and maintenance. The Ideate stage consisted of a comparison of alternatives for the ladder frame, side opening, ramp interface, and modular assembly. Subsequently, the selected concept underwent computer-aided drafting (CAD) and was manufactured in full size. Testing covered structural screening, dimensional suitability, commissioning, practical use, and the documentation of major issues for the next design iteration. The Design Thinking activities were limited to engineering problem definition and prototype development. No clinical studies, treatments, or identifiable health data were included. The requirement collection process in this phase only included non-identifying operational information concerning the boarding space, height of the surface, ramp operation, handhold position, roadway conditions, and limitations in the workshop. Future experiments that would include a direct assessment of persons with disabilities will require the necessary ethical approvals, participant instructions, informed consent, and evaluation of accessibility.

2.2 Design Requirements, Ethical Boundaries, and DFM Translation

Table 1 links the main service requirements to the corresponding prototype features. The vehicle was intended for short, Table 1 links the main service requirements to their corresponding features. The vehicle was intended for short, low-speed journeys on a university campus. The main requirements were a six-passenger capacity, wheelchair accessibility, a low anti-slip floor, an approximate 500 kg payload limit, basic low-speed safety apparatus, local manufacturing capabilities, and modular subsystems that could be easily maintained. This table details how the specific requirements are satisfied but should not be interpreted as evidence of compliance with the industry standards. Table 2 lists the design and manufacturing constraints of the university's workshop. The use of commercially available square hollow sections and manual or semi-automatic operations allowed the definition of the manufacturing envelope of the design. The aforementioned restrictions favor straight elements, repeated joints, and plug-in modules over monocoque solutions. Jigs controlled alignment and simplified fabrication of component interfaces, consistent with the authors' previous work on workshop jig development [17]. The derived configuration was based on the expected behavior of the structure and possible manufacturing processes.

Table 1. Key design requirements and their implementation in the prototype

Requirement	Design target/rationale	Implementation in the prototype
Operating class	Intended for limited-speed LSV operation while incorporating the basic safety features expected for low-speed transport.	A speed limiter was incorporated together with lighting and visibility-related accessories.
Passenger capacity	Designed to accommodate six passengers for short-distance shuttle trips within a campus environment.	Multi-row bench seating was provided, with handholds to improve passenger stability and comfort.
Accessibility	The vehicle should support wheelchair access, minimise boarding height and provide a secure, slip-resistant boarding surface.	A detachable access ramp, open-side entry, and a low chequered-plate floor were incorporated into the design.
Payload	A total payload allowance of approximately 500 kg was adopted to accommodate passengers and wheelchair use.	The seating arrangement and wheelchair-access area were configured around the specified payload capacity.
Safety equipment	Provide the essential equipment required for safe low-speed operation.	The prototype includes a windscreen, side mirrors, lights, a horn, a parking brake, and provisions for seat belts.
Manufacturability	Enable local fabrication using methods that are repeatable and minimise unnecessary rework.	The frame uses standard square-tube sections, jig-assisted fit-up, and modular subframes to simplify fabrication and assembly.
Maintainability and cost	Allow straightforward maintenance while keeping material and labour costs transparent and traceable.	Bolt-on accessories, accessible wiring routes and a direct-cost model based on the BOM and labour hours were adopted.

2.3 Mechanical Architecture and Accessibility Features

The CAD model was developed after establishing the key specifications and workshop constraints. The decision to use a welded tubular frame was based on the need for a clear load path beneath the floor without sophisticated forming processes. Seats, side shields, and roof supports can also be easily attached to the frame. Standard square hollow sections were used wherever possible to simplify the cutting, jigging, and fit-up. The principal frame supports the anti-slip floor, and the front frame carries the steering post and suspension components within a compact turning arrangement. At the rear, the wide track and dual wheels provide greater stability when carrying passengers and wheelchairs. The seat bases, shields, and roof supports were treated as secondary frames and could be repaired or replaced without cutting the main frame. The passenger area was arranged with benches along the sides to maintain a clear access path rather than using the

available floor space for additional seating. Handgrips and rails were fitted inside the cabin to support the passengers during boarding and travel.

Mesh panels were used along the open sides of the cabin to provide protection while maintaining easy access for inspections. Mirrors, lights, a windscreen, horn, parking brake, and seatbelt provisions were also installed. The final belt configuration, warning signs, operating speed, and permitted route must be defined through a campus operational risk assessment before regular use. A removable ramp is used to bridge the ground floor height. The ramp consists of a welded frame with a mesh deck to reduce the mass while providing drainage and surface grip. The side opening provides sufficient space for assisted alignment and boarding of the wheelchair. Figure 2 combines the principal CAD views: (a) the overall vehicle concept, (b) the side access and seating arrangement, and (c) the rear ramp-deployment geometry. The present ramp should not be considered service-qualified until higher proof loading, positive locking or retention, wet surface grip, and wheelchair securement have been verified.

Table 2. Institutional workshop constraints and their implications for DFM

Workshop limitation	Engineering constraint adopted	Influence on design decisions
Material stock	Commercial low-carbon square hollow-section steel was used, primarily in 38.1 × 38.1 × 2 mm and 50.8 × 50.8 × 2 mm sections.	Straight structural members and modular subframes were favoured to reduce forming requirements and simplify fabrication.
Cutting and preparation	Members were prepared using manual or semi-manual cutting, followed by deburring, identification, and trial fit-up.	Joint configurations were kept simple and easily accessible so that parts could be prepared and assembled consistently.
Fit-up and alignment	Assembly was carried out on a flat jig surface. Primary datums were tack-welded first, followed by diagonal and squareness checks before final welding.	A ladder-frame configuration was selected because it provides better dimensional control under typical institutional workshop conditions.
Welding capability	GMAW/MIG welding was used, with workmanship and visual inspection guided by the structural-steel principles of AWS D1.1/D1.1M [34].	A balanced welding sequence and intermediate inspection points were used to limit distortion and identify visible weld defects during fabrication.
Inspection tools	Inspection relied mainly on measuring tapes, steel rulers, visual weld checks, and documented inspection points.	The measurements were therefore treated as evidence of prototype-level acceptance rather than formal production certification.
Assembly strategy	Mechanical and electrical systems were integrated in stages, including seats, guards, canopy supports, and other bolt-on components.	Staged assembly helped reduce rework and provided better access for subsequent maintenance and component replacement.
Cost and labour limit	The cost model was based on the BOM, 240 labour hours, a workshop labour rate of MYR 35/h, and 15% overhead.	Design decisions balanced affordability, fabrication time, ease of manufacture, and sufficient robustness for prototype testing.

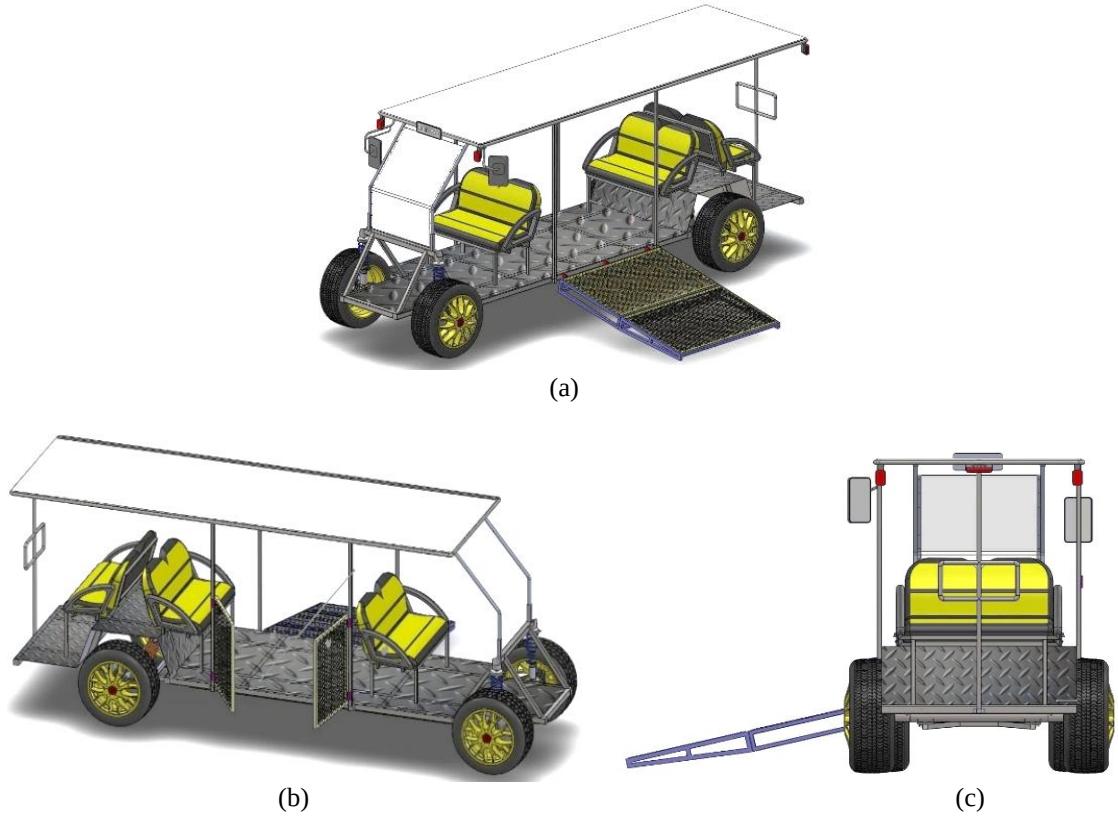
Table 3. Chassis model and finite element analysis settings

Parameter	Specification
Software	SolidWorks Simulation 2021 Education Version
CAD model	Chassis – Raw – Weld Joint (W-O Weld Bead)
Analysis type	Linear static finite element analysis
Unit convention	Geometry and displacement in mm; load in N/kN; stress in MPa
Structural architecture	Tubular ladder-frame chassis
Main tube sections	Square hollow sections of 50.8 × 50.8 × 2 mm and 38.1 × 38.1 × 2 mm
Joint/weld modelling	Weld beads not explicitly modelled; global bonded interactions used
Boundary conditions	Fixed geometry on ten support faces representing the final wheel-support constraints
Applied load	Distributed vertical line load of −1000 N/m applied to four beam entities
Solver settings	Automatic solver; large displacement off; inertial relief off; soft spring off; adaptive method off; free-body force calculation on

2.4 Static Finite Element Analysis of the Ladder-Frame Chassis

Prior to interpreting the prototype results, the ladder-frame chassis was screened using a linear static finite-element model in SolidWorks Simulation 2021 Education Version. The analysis examined the overall deformation pattern, von Mises stress, equivalent strain, support reactions, and yield-based safety margin under a representative vertical service load. This numerical stage complemented the CAD and prototype work by identifying the more flexible regions and areas of concentrated load transfer in the frame. It was not intended to predict fatigue life, crashworthiness, long-term durability,

or roadworthiness. The final model settings are summarised in Table 3. The welded chassis was modelled as a bonded tubular assembly without explicit weld-bead geometry. Fixed geometry was applied to ten support faces at the wheel-support regions, while a distributed vertical line load of −1000 N/m was applied to four beam entities. Large-displacement, inertial-relief and soft-spring options were disabled, and free-body force calculation was retained as an equilibrium check. Figure 3 shows the chassis model, while Figure 4 presents the final load case and the resulting displacement, von Mises stress and factor-of-safety fields.



(a)

(b) (c)

Figure 2. CAD configurations of the wheelchair-accessible campus buggy: (a) overall concept, (b) side-access and seating arrangement, and (c) rear ramp-deployment geometry

The material definitions used in the finite element model are listed in Table 4. The principal members were assigned as AISI 1020 low-carbon steel or an equivalent commercial mild-steel hollow section using a linear-elastic isotropic material model. The yield strength was used as the reference for the von Mises factor-of-safety calculation because the analysis was restricted to the elastic service-load screening. The final discretization is summarized in Table 5. A high-quality blended curvature-based mixed mesh generated 41,571 nodes and 20,772 elements with maximum and minimum element sizes of 21.8015 mm and 1.53073 mm, respectively. This mesh was used for the reported results. The original analysis did not include a formal multilevel mesh convergence series, and adaptive refinement was disabled. Therefore, the FEA results are used to describe the global structural response and identify regions for design attention, rather than as mesh-independent estimates of local weld toe stress or fatigue behavior.

Table 4. Material properties used for the finite element model

Property	Value	Unit
Material	AISI 1020 low-carbon steel	–
Material model	Linear elastic, isotropic	–
Failure criterion	Maximum von Mises stress	–
Elastic modulus, E	200	GPa
Poisson's ratio, ν	0.29	–
Density, ρ	7,900	kg/m³
Shear modulus, G	77	GPa
Yield strength, σ_γ	351.571	MPa
Ultimate tensile strength, σ_u	420.507	MPa

Table 5. Mesh settings and discretisation details used in the finite element analysis

Mesh parameter	Setting/result
Mesh formulation	Mixed-element mesh
Meshing method	Blended curvature-based meshing
Mesh quality setting	High
Jacobian evaluation points	16
Maximum element size	21.8015 mm
Minimum element size	1.53073 mm
Total number of nodes	41,571
Total number of elements	20,772
Adaptive refinement	Off
Mesh-convergence assessment	No formal multi-level convergence series; final mesh used for global structural screening

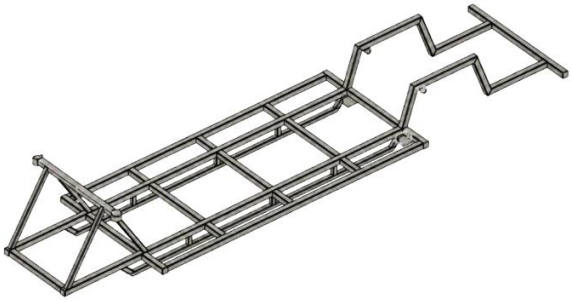


Figure 3. Ladder-frame chassis model used for finite element analysis

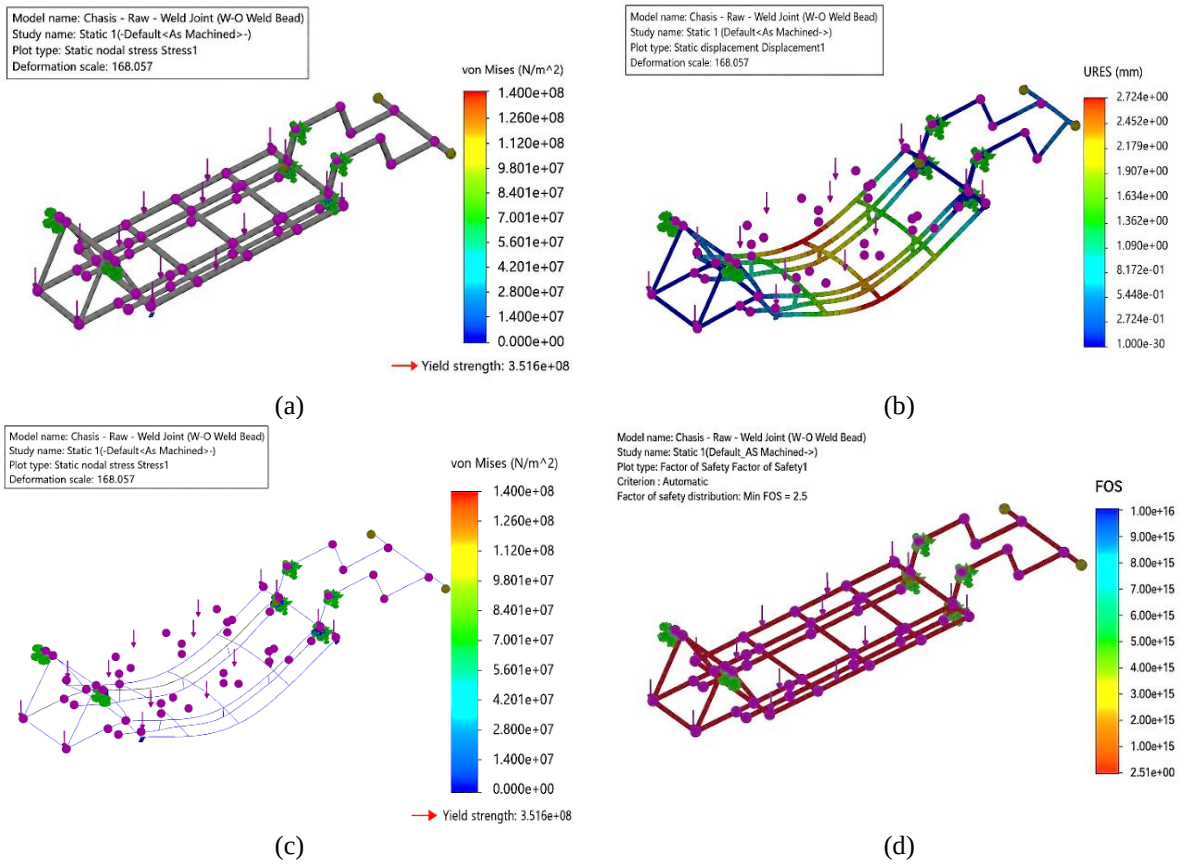


Figure 4. Finite-element model and structural response: (a) static nodal stress plot with applied boundary conditions and loading, (b) resultant displacement, (c) von Mises stress, and (d) factor of safety

The displacement, stress, strain, and safety factor fields were considered together rather than being represented by a single maximum value. Figure 4 shows these differences: the displacement plot reveals the more flexible parts of the

structure, whereas the stress and safety factor plots show more concentrated load-transfer points related to the structure's joints and connections. The visual deformation in SolidWorks is exaggerated and may not represent reality; the practical displacement size was taken from the numerical value rather than the visual one.

2.5 Prototype Fabrication and Assembly

The institution's workshop fabricated the buggy using the available equipment. The main fabrication activities included tube cutting and preparation, drilling, jig-assisted fit-up, gas metal arc welding/metal inert gas (GMAW/MIG) welding, surface preparation, coating, and final mechanical and electrical assembly of the system. The team controlled the weld preparation and tack sequences and visually inspected the completed welds with reference to AWS D1.1/D1.1M [34]. These inspections improved the consistency across the fabrication stages of the research prototype; however, they did not constitute road-vehicle chassis certification.

2.5.1 Manufacturing workflow

The fabrication involved a series of checks before the parts were installed. The tubular members were cut and numbered according to the CAD cut list prior to assembly. The main frame was first tack-welded to check the diagonals, squareness, and critical mounting points before full welding. After verifying the measurements, the team completed the full welding, followed by the installation of the floor plate and brackets. Four inspection points were used during fabrication: fit-up, post-weld visual inspection, post-coating inspection, and final pre-assembly check. This approach minimizes the risk of late-stage dimensional issues and provides a record of the prototype fabrication process.

2.5.2 Surface finishing and staged integration

The finishing and final integration occurred in stages rather than in a single step. The steelwork was mechanically cleaned, sharp edges were rounded, and weld spatter was removed before painting and coating. The front body panel was finished separately to facilitate handling and inspection. The mechanical integration process began with the running gear and mounting points, followed by the traction battery, controllers, cable routing, and electrical protection systems. Seats, guards, canopy components, and controls were fitted after verifying the functional systems. The electrical testing covered fuses, contactor operation, cable identification, insulation status, grounding, and strain relief. Finally, the steering system, emergency brakes, lights, horn, and speed limiters were evaluated. The prototype was completed after the integration of the main body and mechanical components, as shown in Figure 5. Figure 5(a) shows the front view of the vehicle, including the windscreen, front body panel, lighting arrangement, canopy structure, and overall width of the buggy. The image also shows the appearance of the prototype after the installation of the main exterior components. The side view in Figure 5(b) shows the low-floor arrangement, multirow seating, open side-access area, side guards, canopy supports, and overall running-gear positioning. Together, the two views illustrate how accessibility-related features were incorporated into the final vehicle configuration.



(a) (b)

Figure 5. Completed prototype after body-panel integration: (a) front view, and (b) side view

Figure 6 shows the various stages of prototype fabrication, assembly, and deployment. Figure 6(a) presents the body-panel finishing stage, where the front body section is prepared separately from the chassis before the final installation. Figure 6(b) shows the frame during workshop assembly, including the ladder-frame structure and integration of the main structural and mounting components before completion of the vehicle. Figure 6(c) shows the prototype during on-site commissioning, where basic functional checks were performed before the demonstration. Figure 6(d) shows the rear view of the buggy during the demonstration stage, representing the completed vehicle after its fabrication and assembly. Together, these images show the progression from workshop fabrication to a completed prototype for a controlled functional evaluation.



(a)



(b)



(c)



(d)

Figure 6. Prototype fabrication and deployment stages: (a) body-panel finishing, (b) frame assembly, (c) on-site commissioning, and (d) rear view during demonstration

3. Results and Discussion

The buggy was tested after assembly to determine whether it met the expectations established during the design stage. The results are presented in three sections: finite-element analysis, prototype cost analysis, and measurements from the physical prototype. These results illustrate the performance achieved under the conditions investigated in this study and highlight areas for improvement in the next design iteration.

3.1 Finite Element Structural Analysis

The final static analysis showed no indications of member failure. The highest stresses were concentrated around specific joints and member intersections in the structure. The maximum von Mises stress was 140.0 MPa, and the maximum resultant displacement was 2.724 mm. The minimum factor of safety was 2.511 and occurred at the same location as that of the maximum stress. The total support reaction was 11.216 kN, with a dominant vertical component, as shown in Table 6.

Table 6. Summary of finite element output

Output	Minimum/lower result	Maximum/governing result
Von Mises stress, σ_v	0 MPa	140.0 MPa
Resultant displacement, U_{res}	0 mm	2.724 mm
Equivalent strain, ε_{eq}	0	4.521×10^{-4}
Factor of safety	Minimum 2.511	Large non-governing values in near-zero-stress regions
Resultant reaction force	–	11.216 kN, dominant Y component

Resultant displacement was calculated using Eq. (1):

$$U_{res} = \sqrt{U_x{}^2 + U_y{}^2 + U_z{}^2} \quad (1)$$

where Ures denotes resultant displacement and Ux, Uy, and Uz are the three displacement components. For the ductile steel frame, the yield check was based on von Mises equivalent stress. The corresponding safety factor is defined by Eq. (2).

$$FoS = \frac{\sigma_y}{\sigma_{v,max}} \quad (2)$$

where FoS is the factor of safety, σy is the material yield strength, and σv,max is the maximum von Mises stress. Using σy = 351.571 MPa and σv,max = 140.0 MPa gives Eq. (3).

$$FoS = \frac{351.571}{140.0} = 2.511 \quad (3)$$

The value calculated using Eq. (3) agrees with the minimum factor of safety reported by SolidWorks. For this load case, the governing stress remained well below the assigned yield strength, indicating an elastic safety margin of approximately 2.51. Nevertheless, this result should be interpreted within the limits of the model. The joints were treated as bonded connections rather than explicit welds, and the analysis did not include braking, traction, wheel articulation, impact, or fatigue loading. Therefore, FEA is evidence for structural screening and design refinement, not a vehicle certification result. Based on the numerical pattern, future modifications should be applied selectively rather than uniformly throughout the frames. Increasing the sizes of all members would only result in adding extra mass without guaranteeing that the joints undergoing the highest localized demands would be modified adequately. Short gussets, good member continuity, and local stiffening at the most vulnerable joint connections are better candidates for further design improvements. In addition, the zone with the maximum displacement of 2.724 mm should be monitored separately from the stress-critical joints, because stiffness and strength may not occur in the same location.

3.2 Cost and Economic Evaluation

Direct cost was calculated from purchased materials and components, fabrication consumables, labour and overhead. Summing the itemised bill of materials in Table 7 gives MYR 23,220.14. The baseline also includes 240 labour hours at MYR 35/h, equivalent to MYR 8,400.00. Applying 15% overhead to the combined BOM and labour gives MYR 4,743.02, resulting in a corrected direct prototype cost of MYR 36,363.16. The total cost was calculated using Eq. (4):

$$C_T = (C_B + C_L)(1 + r_o) \quad (4)$$

where CT is the total direct prototype cost, CB is the BOM cost, CL is the labour cost, and ro is the overhead rate. The local sensitivity of total cost to an individual component cost, Ci, is given in Eq. (5).

$$\frac{\partial C_T}{\partial C_i} = 1 + r_o \quad (5)$$

Table 7. Bill of materials and estimated cost of the prototype

Subsystem	Component	Specification	Quantity	Unit cost (MYR)	Subtotal (MYR)
Chassis and floor	Square steel tube	AISI 1020 or equivalent SHS, 38.1 × 38.1 × 2 mm and 50.8 × 50.8 × 2 mm	99 m	11.67	1,155.33
Chassis and floor	Floor plate	Mild-steel chequered plate, 1524 mm × 3048 mm × 3.0 mm	1 sheet	713.43	713.43
Body and canopy	Roof panel	Polycarbonate/ACP roof panel	1	400.00	400.00
Body and canopy	Front body panel	FRP or formed front body panel	1	800.00	800.00
Safety and guards	Side mesh guards	Expanded-metal or mesh side guards	1 lot	400.00	400.00
Accessibility	Detachable ramp	Welded ramp frame with mesh deck and latch	1	300.00	300.00
Seating and interior	Passenger seats	Cushioned passenger bench-seat set	1 set	800.00	800.00
Running gear	Wheels and tyres	Complete wheel-and-tyre set	1 set	1,200.00	1,200.00
Running gear	Suspension set	Shock absorbers and associated mountings	1 set	1,500.00	1,500.00
Running gear	Steering system	Steering and brake-related components	1	800.00	800.00
Drivetrain	Traction motor	5 kW traction motor, 48–72 V class	1	2,064.42	2,064.42
Drivetrain	Motor controller	72 V, 5 kW motor controller	1	415.96	415.96
Energy storage	Battery pack	72 V, 150 Ah $LiFePO_4$ battery pack with BMS	1	10,221.00	10,221.00
Energy storage	On-board charger	72 V charger, approximately 20 A	1	300.00	300.00
Electrical	Wiring and protection	Wiring harness, fuses, contactor, and electrical protection	1 lot	600.00	600.00
Electrical	Lights and horn	Front/rear lighting and horn set	1 lot	250.00	250.00
Finishing	Paint and coating	Primer, paint, and coating materials	1 lot	500.00	500.00
Others	Fasteners and brackets	General fasteners and fabricated brackets	1 lot	300.00	300.00
Fabrication	Consumables	Welding wire, shielding gas, cutting/ grinding discs, and related consumables	1 lot	500.00	500.00
Total					23,220.14

The dimensionless cost elasticity used to compare the influence of components is given by Eq. (6).

$$E_i = \frac{(1 + r_o)C_i}{C_T} \tag{6}$$

where E_i represents the cost, elasticity associated with component i, and C_i represents the corresponding baseline component cost. This form of calculation is useful when the cost estimate needs to be updated because a change in the battery price, drivetrain cost, or fabrication time can be carried through to the total without rebuilding the entire model. The BOM in Table 7 clarifies the component cost concentration. The 72 V, 150 Ah $LiFePO_4$ battery pack was the largest single purchase at MYR 10,221.00. The next largest items are the 5-kW traction motor at MYR 2,064.42, suspension set at MYR 1,500.00, and wheel-and-tire set at MYR 1,200.00. The frame and floor account for a smaller share because they are primarily made from standard mild-steel tubes and plates.

Workshop labor was concentrated mainly in the welding stage, which accounted for 70 of the estimated 240 labor-hours. This reflects the number of joints, welding sequence, and need to maintain access for local repairs. Electrical integration also requires substantial time because the components must be installed, wired, protected, labelled, and functionally checked. For future builds, labor savings are more likely to come from improving the jigs, cut lists, component interfaces, and assembly sequence than from increasing the welding speed alone.

Table 8. Estimated labour requirements for prototype fabrication and assembly

Activity	Main tasks	Estimated labour (h)	Remarks
Cutting and preparation	Tube cutting, deburring, member identification, and mitre cutting	20	Varies with the number of frame members and available cutting equipment
Fit-up and tack welding	Jig setup, dimensional alignment, and tack welding	25	Establishes the main frame geometry and helps control welding distortion
Full welding	Completion of structural welds and local rework where required	70	Largest single labour requirement in the fabrication process
Grinding and surface preparation	Weld-spatter removal, edge finishing, and surface preparation	20	Prepares the structure for coating and improves surface finish
Coating and painting	Primer and top-coat application, including curing time	10	May be outsourced where appropriate
Floor and bracket installation	Installation of the floor plate, seat bases, and mounting brackets	15	Bolt-on interfaces help minimise subsequent rework
Ramp fabrication	Fabrication of the ramp frame, mesh deck, and latch	10	Includes preparation for the prototype load test
Electrical integration	Installation of the battery, motor controller, wiring, and electrical protection	35	Includes cable routing, labelling, and protection checks
Final assembly	Installation of seats, guards, canopy, and accessories	25	Includes fit-up and fastening checks
Commissioning	Functional inspection and low-speed shakedown testing	10	Used to document and verify the final as-built configuration
Total		240	Equivalent labour cost: MYR 8,400 at MYR 35/h

Table 9 lists the principal cost drivers based on a revised direct cost baseline. A 20% reduction in battery pricing decreases the total direct cost by MYR 2,350.83, which is equivalent to 6.46%. A similar 20% decrease in working hours reduces the total cost by MYR 1,932.00, or 5.31%. The same decrease applied to the motor and controller leads to a decrease of MYR 570.49 or 1.57% in the total cost. For the same build, battery acquisition offers the most immediate opportunity to reduce direct costs, whereas workshop labour is the next significant area to improve. On a smaller fleet scale, the team expects more effective jigs, numerous subassemblies, established wiring instructions, and earlier inspection points to minimise the assembly time while achieving better manufacturing consistency across different vehicles.

Table 9. Summary of formal cost sensitivity

Cost group	Baseline value (MYR)	Elasticity	Scenario	Change in total cost (MYR)	Interpretation
Battery pack	10,221.00	0.3232	20% reduction	2,350.83	6.46% reduction in total cost
Labour hours	8,400.00	0.2657	20% reduction	1,932.00	5.31% reduction in total cost
Motor and controller	2,480.38	0.0784	20% reduction	570.49	1.57% reduction in total cost
BOM excluding battery	12,999.14	0.4111	10% reduction	1,494.90	4.11% reduction in total cost

3.3 Prototype Validation and Experimental Evaluation

Verification by the physical prototype followed the assembly and commissioning of the vehicle. The checks included the dimensions of the frame, loading of the ramp, stopping distance, side slope performance, mechanical and electrical basic functionalities, and the use of batteries, including charging and the output of the photovoltaic panel on the roof.

Verification was performed under controlled prototype conditions, and the results were presented as engineering observations for a particular phase of development.

3.3.1 Dimensional verification of the manufactured frame

The frame dimensions were checked before painting and final assembly to identify any welding-induced distortion. A tape measure and steel ruler were employed to check the two main diagonals, validate the squareness of the cross members, and verify certain mounting interfaces. The as-built measurements used for the inspection are listed in Table 10. The diagonals measured 2688 and 2693 mm, yielding a variation of 5 mm or approximately 0.19% of the diagonal 2.69 m. The frame could still be assembled with its primary parts without issues; thus, this variation was accepted for this prototype. This acceptance was a decision made by the workshop in the case of unit production and should not be interpreted as official vehicle tolerance. If the design is produced again, the limits on length, angle, and flatness should be specified directly in the drawings and inspection sheets. The ISO 2768-1 can be used as a general guide whenever there is no individual tolerance [35].

Table 10. Dimensional verification of the fabricated chassis

Measurement	Design target	Measured value	Assessment
Frame diagonal A	–	2688 mm	Reference measurement
Frame diagonal B	–	2693 mm	+5 mm relative to diagonal A
Cross-member squareness difference	Internal prototype limit ≤ 6 mm	5 mm	Within the prototype acceptance limit
Seat-base hole spacing	320 mm	319 mm	−1 mm
Rear-axle mount alignment	–	Within 2 mm	Recorded as-built dimension
Floor-interface height	–	420 mm	Recorded as-built value

3.3.2 Ramp static load test

The detachable ramp was situated in the same location that was used for boarding during the ramp test and loaded in increments. Calibrated masses were placed at mid-span, where the greatest bending was expected. Each load was held for two minutes before the deflection was measured. After each deflection reading, the load was removed and the ramp was measured again to distinguish residual deformation from elastic recovery. The three load increments and their respective deflections can be seen in Table 11. The ramp deflected by 8.6 mm under the 180 kg test load and retained 0.4 mm residual displacement after unloading, with no visible failure. This indicates satisfactory elastic behaviour under the prototype test condition, but it is insufficient to define a universal service rating because the combined mass of a powered wheelchair and an adult may exceed 200 kg. Higher proof loads and verification of the locking mechanism are therefore required before practical use.

Table 11. Ramp static load test results

Load case	Applied load (kg)	Hold time (min)	Maximum deflection (mm)	Residual deflection (mm)	Observation
Test 1	120	2	4.2	0.1	No visible damage
Test 2	150	2	6.3	0.2	Ramp position stable
Test 3	180	2	8.6	0.4	Elastic bending only

3.3.3 Ramp deployment usability test

Ramp handling was evaluated over five deployment and stowage cycles to assess whether the detachable ramp could be positioned and removed within a practical operating time under dry conditions. Mean deployment and stowage times were 18 s and 16 s, respectively. No unintended release or slip was observed on the dry test surface. Because the assessment covered only five cycles and one surface condition, the result demonstrates handling feasibility rather than long-term reliability.

Table 12. Ramp deployment and handling assessment

Assessment parameter	Observed result
Mean deployment time	18 s
Mean stowage time	16 s
Number of deployments–stowage cycles	5
Ramp stability during deployment	No unintended movement or release observed
Slip on dry surface	None observed

3.3.4 Braking performance test

The buggy was driven on a dry, level, paved surface and brought to a stop from an indicated speed of approximately 15 km/h. Tests were conducted with the driver only, with a partial load, and with the full test load, and three stops were recorded for each condition. The driver began braking at a fixed visual marker, and the distance to rest was measured.

Because the procedure relied on a human trigger and manual distance measurement, the figures included normal response time and marker-reading uncertainty. Therefore, they should be them as practical stopping distances for the prototype rather than instrumented brake-system measurements.

Table 13. Measured stopping distance under different payload conditions

Load condition	Test speed (km/h)	Payload (kg)	Trial 1 (m)	Trial 2 (m)	Trial 3 (m)	Mean stopping distance (m)
Driver only	15	85	3.8	3.9	4.0	3.9
Partial load	15	250	4.6	4.8	4.7	4.7
Full load	15	420	5.3	5.4	5.5	5.4

The mean stopping distance increased from 3.9 m with the driver alone to 5.4 m under full-load conditions. At 15 km/h, the initial speed was 4.167 m/s. Assuming a constant average deceleration, the corresponding estimate can be obtained from Eq. (7).

$$a = \frac{v^2}{2d} \tag{7}$$

Substituting v = 4.167 m/s and d = 5.4 m gives:

$$a = \frac{(4.167)^2}{2 \times 5.4} = 1.61\ m/s^2 \tag{8}$$

The calculated average deceleration is approximately 0.164 g. The consistent increase in stopping distance with payload supports conservative speed control on campus routes, but the test should not be interpreted as a regulatory emergency-braking assessment. Recent IJAME work on electric-vehicle longitudinal performance likewise used measured speed, travel distance, motor variables and battery voltage to strengthen dynamic validation [36]. Future testing of this prototype should use a pedal trigger, wheel-speed sensing, GPS/IMU logging or optical timing gates.

3.3.5 Static stability assessment

Static lateral stability was examined by gradually inclining the vehicle until initial wheel lightening was observed. This point was used as a practical indicator of incipient rollover under quasi-static conditions. Driver-only and loaded configurations were tested, and the results are reported in Table 14.

Table 14. Static lateral slope stability results

Condition	Payload (kg)	Side-slope angle at initial wheel lightening	Stability assessment
Driver only	85	24°	Stable under tested conditions
Loaded	420	21°	Stable under tested conditions

A simple rigid-body model was used only to interpret the observed wheel-lightening angle. For a laterally centred centre of gravity, the critical side-slope angle is given by Eq. (9).

$$\theta_c = tan^{-1}\left(\frac{T/2}{h_{CG}}\right) \tag{9}$$

where θc is the critical side-slope angle, T is the effective track width and hCG is the centre-of-gravity height. If the centre of gravity is laterally offset, yCG is introduced as shown in Eq. (10).

$$\theta_c = tan^{-1}\left(\frac{T/2 - y_{CG}}{h_{CG}}\right) \tag{10}$$

The 21° wheel-lightening angle measured with the vehicle loaded describes the particular arrangement tested, but it is not certified as a rollover angle. The passenger location, wheelchair mass, and positions of heavy components, such as the battery, will all shift the centre of gravity. Therefore, a service limit should not be established based solely on this test. The next stability study should measure the centre of gravity directly, repeat the test with representative load positions and include dynamic turning and braking conditions

3.3.6 Functional commissioning tests

electrical systems operated as intended. The checks covered forward and reverse control, throttle response, steering operation, service and parking brakes, lighting, horn function, battery indication, and cable routing. Table 15 summarizes the outcomes. All systems listed in Table 15 operated satisfactorily under the test conditions of this study. These results support the supervised low-speed demonstration of the prototype on a controlled campus route. However, they should be regarded as prototype-level functional verifications rather than approvals for unsupervised operation or use on public roads.

Table 15. Functional verification of the main vehicle systems

System	Verification check	Observed result
Directional control	Forward and reverse operation	Pass
Throttle response	Smooth and progressive acceleration	Pass
Steering system	Full steering range achieved without interference	Pass
Service brake	Vehicle stopped effectively during the functional check	Pass
Parking brake	Vehicle remained stationary on the test slope	Pass
Lighting system	Front and rear lights operated correctly	Pass
Horn	Audible warning signal operated correctly	Pass
Battery indicator	State-of-charge display operated correctly	Pass
Cable routing	No visible interference, abrasion or loose routing	Pass

3.3.7 Battery energy consumption and range assessment

Battery energy use was assessed during repeated stop–start operations on a paved campus route at an average speed of approximately 18 km/h. The vehicle was powered by a 72 V, 150 Ah battery pack with a nominal energy capacity of approximately 10.8 kWh. Energy consumption was estimated from the reduction in the state of charge (SOC) shown by the onboard display, whereas a 90% usable energy fraction was assumed to retain an operating reserve when estimating the range. The results for the driver-only and full-load operations are listed in Table 16. A recent study on battery-electric vehicle structures also highlighted the close relationship between battery packaging and overall vehicle architecture [37]. The estimated specific energy consumption increased from 184 Wh/km with the driver alone to 238 Wh/km under full load, reducing the corresponding estimated range from 52.8 to 40.8 km. The direction of change is physically consistent with a higher rolling resistance, repeated acceleration demand, and drivetrain loading associated with a greater payload. These values should be treated as planning estimates rather than high-accuracy energy measurements.

Table 16. Battery energy consumption and estimated range at approximately 18 km/h

Condition	Average speed (km/h)	Payload (kg)	Distance (km)	SOC drop (%)	Energy used (kWh)	Specific consumption (Wh/km)	Estimated range (km)
Driver only	18	85	10.0	17	1.84	184	52.8
Full load	18	420	10.0	22	2.38	238	40.8

Experimental battery studies have shown that the discharge response and thermal state vary with the load and operating conditions [38], whereas electric-vehicle energy-source research emphasizes the importance of matching the storage characteristics to the duty cycle [39]. Dynamic battery modelling also shows why state estimation is sensitive to the applied current profile [40]. A more rigorous assessment of this prototype should continuously record the voltage and current using a calibrated shunt, Hall-effect sensor, or power analyzer.

$$E = \int V(t)\, I(t)\, dt \tag{11}$$

where E is electrical energy, V(t) is instantaneous battery voltage and I(t) is instantaneous battery current. Direct integration would provide a stronger basis for Wh/km estimation, route-energy prediction and battery sizing.

3.3.8 On-board charging performance test

presents the observed increase from 20% to 100% SOC. The SOC increased from 20% to 100% in approximately 6 h. This duration is compatible with overnight campus charging, provided that the charging location, electrical protection, ventilation, supervision, and battery management procedures are defined. Routine operations should also include battery temperature and charging history records.

Table 17. Charging-time profile using the on-board charger

Time from start (h)	SOC (%)
0.0	20
1.0	35
2.0	50
3.0	65
4.0	78
5.0	90
6.0	100

3.3.9 Roof-mounted solar panel performance test

The roof-mounted photovoltaic (PV) system was measured outdoors to estimate its supplementary contribution to the energy system of the vehicle. Table 18 summarises the voltage, current, and calculated power recorded three times a day. Using an effective average output of approximately 135 W over six sun-hours yields approximately 0.81 kWh/day, which

is equivalent to approximately 7–8% of the nominal 10.8 kWh battery capacity. At an estimated consumption of 184–238 Wh/km, this contribution corresponds to approximately 3–4 km of additional range before charging losses are considered. Therefore, the roof-mounted PV system should be regarded as a supplementary energy source rather than the primary means of charging the vehicle.

Table 18. Roof-mounted PV output measurements under outdoor lighting conditions

Time	Vpv (V)	Ipv (A)	Ppv (W)	Condition
11:00	33.0	4.7	155	Bright sunlight
13:00	33.5	5.4	181	Peak sun
15:00	32.2	3.9	126	Partly cloudy

Using an effective average output of approximately 135 W over six sun-hours gives about 0.81 kWh/day, equivalent to roughly 7–8% of the nominal 10.8 kWh battery capacity. At the estimated consumption of 184–238 Wh/km, this contribution corresponds to approximately 3–4 km of additional range before charging losses are considered. The roof-mounted PV system should therefore be regarded as a supplementary energy source rather than the primary means of charging the vehicle.

3.3.10 Discussion

The project shows that accessibility requirements can be incorporated into the mechanical design without making the vehicle impractical for fabrication in a university workshop. Standard square hollow sections, repeated joints, and jig-assisted fit-up were suited to the available processes, whereas the low floor, side opening, and detachable ramp were retained within a relatively simple ladder frame layout. The structural response of the final chassis configuration was evaluated using finite element analysis. Under the prescribed static vertical load, the maximum von Mises stress was 140.0 MPa, and the minimum safety factor was 2.511. This value indicates that the chassis remained within the elastic range for the load case. However, these results cannot be considered representative of all the operating conditions. The stress distribution identified several joints and member intersections as highly loaded regions. This may require local reinforcement or improvements to ensure the continuity of the members. Next, fatigue evaluation and physical verification of the numerical response are necessary for structural analysis. This study aims to consider asymmetric wheel loading, torsion, braking, and traction loads, as well as detailed weld modelling. In general, the physical test results supported the numerical evaluation.

However, this is insufficient to prove that the prototype is ready for routine service. The ramp returned almost completely to its original state after the 180 kg load test. The stopping distance also increased with the load. The findings showed that the wheel began to lift during the side slope test. These findings are useful for future design improvements. However, this is insufficient for unrestricted operations. This includes ramp tests at higher proof loads, the provision of positive locking mechanisms and wheelchair restraint systems, instrumented braking tests, and direct centre-of-gravity measurements. The energy and cost results can be used as a basis for future planning. The estimated energy consumption at full load was approximately 29% higher per kilometre than that without passenger. The charging time was compatible with overnight charging. Photovoltaic panels mounted on the roof provide only a small amount of additional energy to the building. The direct cost of the revised prototype was MYR 36,363.16, with the battery pack and labour being the largest contributors. Based on the available evidence, the prototype is suitable for further testing on campus under controlled conditions. However, it is not yet ready for routine clinical use.

4. Conclusions

A functional prototype of an electric vehicle, specifically adapted for wheelchair access, was developed. The design and layout of the fabrication were performed using the resources available in the institution workshop. It has easily accessible multi-row seating with side guards, a lightweight canopy, and removable ramps. The frame was low, with side access. It was designed for workshop fabrication with repeatable joints for future repair. For the static load case analysed, the chassis had a maximum von Mises stress of 140.0 MPa with a maximum resultant displacement of 2.724 mm, equivalent strain of 4.521×10^{-4}, and minimum factor of safety of 2.511. The joints and intersections of the members were where most of the stress was concentrated. These areas will require attention in future designs. The corrected direct cost of the prototype was MYR 36,363.16. This included MYR 23,220.14 for BOM, MYR 8,400.00 for labour, and MYR 4,743.02 for overhead. Dimensional inspection revealed a 5 mm difference between the two frame diagonals. The ramp response remained highly elastic for loads up to 180 kg. At a speed of 15 km/h, the stopping distance varied from 3.9 m to 5.4 m, depending on the load condition. The initial wheel unloading occurred at angles of 24° (driver-only) and 21° (loaded). All major functional tests were successfully completed. The operating range was estimated to be approximately 52.8 km (driver-only) and 40.8 km with a full load. Charging the battery from 20% to 100% took approximately 6 h. These results provide additional evidence for the continued development of controlled prototypes. Currently, the results do not justify the certification for routine use. Before operational use, other improvements should include higher ramp proof-load testing, positive locking mechanisms, formal wheelchair restraint systems, instrumented braking and energy consumption measurements, direct measurement of the centre of gravity, fatigue and torsional strength tests, durability tests along the operating route, wet-grip evaluation, corrosion protection, and thorough weld inspection.

Acknowledgements
The authors acknowledge Universiti Sultan Zainal Abidin (UniSZA) for the technical support and access to research facilities. The authors also acknowledge the Department of Mechanical and Production Engineering, Islamic University of Technology, Bangladesh, for the research facilities, technical support, and institutional assistance provided during this study.

Funding
This work was supported by the Ministry of Higher Education Malaysia and Universiti Sultan Zainal Abidin (UniSZA) through the Fundamental Research Grant Scheme for Early Career Researchers (FRGS-EC), Grant No. FRGS-EC/1/2024/TK10/UNISZA/02/3.

Declaration of Competing Interests
The authors declare no relevant financial or non-financial conflicts of interest.

CRediT Author Contribution Statement
Zammeri Abd Rahman: Conceptualisation; Methodology; Validation; Supervision; Project administration; Funding acquisition; Writing – review & editing.
Saiful Bahri Mohamed: Methodology; Formal analysis; Validation; Project administration; Writing – review & revise
Rodianah Alias: Methodology; Data curation; Validation; Investigation; Writing – review & revise
Mohd Sobri Hamid: Investigation; Resources; Data curation; Visualisation; Writing – review & revise
Mohd Shahir Kasim: Software; Analysis; Validation; Visualisation; Writing – review & revise
W Noor Fatihah W. Mohamad: Investigation; Data curation; Validation; Writing – review & revise
Wan Ahmad Luqman Ellias Wan Saidi: Investigation; Data curation; Validation; Writing – review & revise
Ahmad Syauqi Azlan: Conceptualisation; Methodology; Software; Validation; Writing – review & revise
Madihah Maharof: Software; Formal analysis; Validation; Visualisation; Writing – review & revise

Availability of Data and Materials
The datasets generated and/or analyzed during the current study are available from the corresponding author upon reasonable request.

Ethics Statement
This study did not involve human participants or animal subjects, and no identifiable personal data were collected or analysed. The work was limited to engineering design, simulation, prototype fabrication and controlled engineering verification. Ethical approval was therefore not required for this research.

Generative Artificial Intelligence Disclosure
OpenAI ChatGPT was used during manuscript revision to assist with language editing, grammar refinement, consistency checking, reference-format checking and reorganisation of text in response to editorial comments. No generative artificial intelligence tool was used to generate research data, conduct the reported engineering analyses, fabricate experimental results, or determine the scientific conclusions.

References
[1] C. Fleet and O. Kondrashov, "Universal design on university campuses: A literature review," *Exceptionality Education International*, vol. 29, no. 1, pp. 136-148, 2019, https://doi.org/10.5206/eei.v29i1.11125.
[2] L.-O. Losinsky, T. Levi, K. Saffey, and J. Jelsma, "An investigation into the physical accessibility to students who use wheelchairs of an institution of higher education in South Africa," *Disability and Rehabilitation*, vol. 25, no. 7, pp. 305-308, 2003, https://doi.org/10.1080/0963828021000043743.
[3] S. Hayat and V. Fast, "Classifying and mapping accessible mobility on post-secondary campuses," *Spatial Knowledge and Information Canada*, vol. 7, no. 5, Art. no. 3, 2019.
[4] National Highway Traffic Safety Administration, 49 CFR 571.500, Standard No. 500; Low-speed vehicles, U.S. Department of Transportation. [Online]. Available: https://www.ecfr.gov/current/title-49/section-571.500. [Accessed: 04-Jul-2026].
[5] National Highway Traffic Safety Administration, TP-500-02: Laboratory Test Procedure for FMVSS No. 500 Low-Speed Vehicles. Washington, DC, USA: U.S. Department of Transportation, 2006.
[6] S. Akter, M. M. H. Mamun, J. L. Mwakalonge, G. Comert, and S. Siuhi, "A policy review of electric personal assistive mobility devices," *Transportation Research Interdisciplinary Perspectives*, vol. 11, p. 100426, 2021, https://doi.org/10.1016/j.trip.2021.100426.
[7] N. Bray, J. Noyes, R. T. Edwards, and N. Harris, "Wheelchair interventions, services and provision for disabled children: A mixed-method systematic review and conceptual framework," *BMC Health Services Research*, vol. 14, p. 309, 2014, https://doi.org/10.1186/1472-6963-14-309.
[8] J. Pearlman, R. Cooper, H. S. Chhabra, and A. Jefferds, "Design, development and testing of a low-cost electric powered wheelchair for India," *Disability and Rehabilitation: Assistive Technology*, vol. 4, no. 1, pp. 42–57, 2009, https://doi.org/10.1080/17483100802338440.

[9] D. Lee and S. Kim, "Design and control of a novel detachable driving module for electrification of manual wheelchairs," *IEEE Access*, vol. 11, pp. 10169-10179, 2023, https://doi.org/10.1109/ACCESS.2023.3240465.
[10] I. A. Galkin, R. Geidarovs, and A. Podgornovs, "Modular segmented motor for power-assist wheelchairs: Proof of concept," *Machines*, vol. 9, no. 10, Art. no. 227, 2021, https://doi.org/10.3390/machines9100227.
[11] I. Thomas, M. I. John, R. Lal, J. Lukose, and J. Sanjog, "Design and fabrication of low-cost detachable power unit for a wheelchair," in *Advances in Electromechanical Technologies, Lecture Notes in Mechanical Engineering*. Singapore: Springer, 2021, pp. 755-764, https://doi.org/10.1007/978-981-15-5463-6_67.
[12] S. Magibalan, C. Ragu, D. Nithish, C. Raveeshankar, and V. Sabarish, "Design and fabrication of electric three-wheeled scooter for disabled persons," *Materials Today: Proceedings*, vol. 74, no. 4, pp. 820-823, 2023, https://doi.org/10.1016/j.matpr.2022.11.179.
[13] M. H. Al-Ajmi et al., "Design and implementation of a smart electric omnidirectional wheelchair using consumer off-the-shelf components," in *Proceedings of the 2023 5th International Conference on Bio-engineering for Smart Technologies* (BioSMART), Paris, France, 2023, pp. 1–5, https://doi.org/10.1109/BioSMART58455.2023.10162066.
[14] T. Brown, "Design thinking," *Harvard Business Review*, vol. 86, no. 6, pp. 84-92, 2008.
[15] G. Boothroyd, P. Dewhurst, and W. A. Knight, *Product Design for Manufacture and Assembly*, 3rd ed. Boca Raton, FL, USA: CRC Press, 2011, https://doi.org/10.1201/9781420089288.
[16] K. T. Ulrich, S. D. Eppinger, and M. C. Yang, *Product Design and Development*, 7th ed. New York, NY, USA: McGraw-Hill Education, 2020.
[17] N. H. Che Amid et al., "Design and development of a universal magnetic portable jig: A modular approach for versatile clamping applications," *Journal of Advanced Research Design*, vol. 125, no. 1, pp. 79-102, 2025, https://doi.org/10.37934/ard.125.1.79103.
[18] A. S. Aziz et al., "Design and development of an electromagnetic portable drill guide for improved precision and efficiency in DIY applications," *Journal of Advanced Research Design*, vol. 126, no. 1, pp. 26-41, 2025, https://doi.org/10.37934/ard.126.1.2641.
[19] Z. Abd Rahman, S. B. Mohamed, A. R. Zulkifli, M. S. Kasim, and W. N. F. Mohamad, "Design and fabrication of a PC-based 3-axis CNC milling machine," *International Journal of Engineering Trends and Technology*, vol. 69, no. 9, pp. 1-13, 2021, https://doi.org/10.14445/22315381/IJETT-V69I9P201.
[20] Z. Abd Rahman et al., "Optimisation of structural design in benchtop CNC milling machines for enhanced performance and efficiency," *Journal of Advanced Research in Applied Mechanics*, vol. 129, no. 1, pp. 57–74, 2024, https://doi.org/10.37934/aram.129.1.5774.
[21] W. Afzal and R. A. Mufti, "Optimal cross-section of cross member for increased torsional and bending stiffness of ladder frame chassis," in *Proceedings of the 2019 16th International Bhurban Conference on Applied Sciences and Technology*, 2019, pp. 218-228, https://doi.org/10.1109/IBCAST.2019.8667195.
[22] H. Rajesh, M. A. Patwardhan, N. V. Karanth, and Y. P. Reddy, "LCV chassis frame optimization using combined simulation and experimental approach," SAE Technical Paper 2017-26-0289, 2017, https://doi.org/10.4271/2017-26-0289.
[23] B. Bhupathi, J. Shivashekar, D. Vamshi, and A. B. Ghubade, "Material analysis of ladder frame chassis for heavy vehicle: A brief review," *AIP Conference Proceedings*, vol. 3185, Art. no. 020005, 2025, https://doi.org/10.1063/5.0245568.
[24] L. M. Barbosa, J. Tomazini, M. Martins, and L. Q. Moreira, "Finite element and experimental analysis of the torsional stiffness of a chassis of a Baja SAE prototype," SAE Technical Paper 2016-36-0124, 2016, https://doi.org/10.4271/2016-36-0124.
[25] N. Noorbhasha and B. J. O'Toole, "Static analysis on a roll cage frame for an off-road vehicle," SAE Technical Paper 2017-01-1299, 2017, https://doi.org/10.4271/2017-01-1299.
[26] M. H. Tullah, D. A. Sumarsono, R. Noval, et al., "Design and evaluation of hollow frame structures for the development of urban-centric two-passenger electric vehicles," *Eastern-European Journal of Enterprise Technologies*, vol. 5, no. 7(125), pp. 80–86, 2023, https://doi.org/10.15587/1729-4061.2023.289232.
[27] S. Balakirupakaran, M. Dharanish, S. Kiran Srinivas, and B. Karunaamoorthy, "Design and development of two-wheel electric vehicle," in *Proceedings of the 2023 International Conference on Intelligent Technologies for Sustainable Electric and Communications Systems* (iTech SECOM), Coimbatore, India, 2023, pp. 259–264, https://doi.org/10.1109/iTechSECOM59882.2023.10434988.
[28] H. Brodin and J. Persson, "Cost-utility analysis of assistive technologies in the European Commission's TIDE program," *International Journal of Technology Assessment in Health Care*, vol. 11, no. 2, pp. 276-283, 1995, https://doi.org/10.1017/S0266462300006899.
[29] S. K. Sahoo and B. B. Choudhury, "Optimal selection of an electric power wheelchair using an integrated COPRAS and EDAS approach based on entropy weighting technique," *Decision Science Letters*, vol. 11, no. 1, pp. 21-34, 2022, https://doi.org/10.5267/j.dsl.2021.10.002.
[30] T.-T. Fu, "A multi-criteria parametric evaluation of the refueling strategies for scooters," *Journal of Engineering Design*, vol. 19, no. 3, pp. 227-247, 2008, https://doi.org/10.1080/09544820701327830.
[31] S. Eduardo, E. A. Recklies, M. Nikolic, and S. Severengiz, "Cost-benefit analysis for end-of-life scenarios: A case study of an electric moped," *Sustainability*, vol. 17, no. 21, Art. no. 9819, 2025, https://doi.org/10.3390/su17219819.

[32] S. Eduardo, E. A. Recklies, M. Nikolic, and S. Severengiz, "A comparative life cycle assessment of end-of-life scenarios for light electric vehicles: A case study of an electric moped," *Sustainability*, vol. 17, no. 15, Art. no. 6681, 2025, https://doi.org/10.3390/su17156681.

[33] K. Saez de Bikuna, M. Pierobon, C. Soldati, M. Vale, and N. Picone, "Repurposing of electric vehicle batteries for second life stationary applications in residential photovoltaic systems: An environmental and economic sustainability assessment," *International Journal of Environmental Research*, vol. 19, Art. no. 119, 2025, https://doi.org/10.1007/s41742-025-00788-6.

[34] American Welding Society, *AWS D1.1/D1.1M:2025 Structural Welding Code - Steel*. Miami, FL, USA: AWS, 2025.

[35] International Organization for Standardization, *ISO 2768-1:1989, General Tolerances - Part 1: Tolerances for Linear and Angular Dimensions without Individual Tolerance Indications*. Geneva, Switzerland: ISO, 1989.

[36] M. S. A. Razak, F. Ahmad, M. H. Che Hasan, and H. Jamaluddin, "Dynamic testing of in-wheel motor based electric vehicle in longitudinal direction," *International Journal of Automotive and Mechanical Engineering*, vol. 20, no. 3, pp. 10574–10594, 2023, https://doi.org/10.15282/ijame.20.3.2023.02.0816.

[37] H. Shafaqat, C. Krüger, and P. Urban, "Parametric analysis of a divided rocker for battery electric vehicles," *International Journal of Automotive and Mechanical Engineering*, vol. 20, no. 1, pp. 10274–10284, 2023, https://doi.org/10.15282/ijame.20.1.2023.09.0794.

[38] D. H. Arthanto, B. Nuryadin, K. P. Sumarah et al., "Discharge and thermal distribution characteristics of electric vehicle battery pack in closed circuit system," *International Journal of Automotive and Mechanical Engineering*, vol. 21, no. 1, pp. 11166–11175, 2024, https://doi.org/10.15282/ijame.21.1.2024.17.0863.

[39] C. Chen and G. Ren, "Modeling and simulation of a battery/supercapacitor hybrid power source for electric vehicles," *International Journal of Automotive and Mechanical Engineering*, vol. 21, no. 2, pp. 11176–11190, 2024, https://doi.org/10.15282/ijame.21.2.2024.1.0864.

[40] M. Yıldız and A. Aktürk, "Battery simulation using the NTGK model: Effects of model parameters and implementation under dynamic current profiles," *International Journal of Automotive and Mechanical Engineering*, vol. 22, no. 3, pp. 12713–12724, 2025, https://doi.org/10.15282/ijame.22.3.2025.14.0971.